Polymer Journal (2018) 50:1169–1177
https://doi.org/10.1038/s41428-018-0108-9

ORIGINAL ARTICLE

Properties and surface morphologies of organic–inorganic hybrid thin films containing titanium phosphonate clusters

Ryohei Hayami[1] · Keisuke Wada[1] · Yuta Miyase[1] · Takuya Sagawa[1] · Satoru Tsukada[2] · Kazuki Yamamoto[1] · Takahiro Gunji[1]

Received: 2 April 2018 / Revised: 27 June 2018 / Accepted: 29 June 2018 / Published online: 27 July 2018

Abstract

Organic–inorganic hybrid thin films containing $[Ti_4(\mu_3\text{-}O)(O\mathit{i}Pr)_5(\mu\text{-}O\mathit{i}Pr)_3(O_3PPh)_3]$·THF (TiOPPh) were prepared via the hybridization of TiOPPh with poly(vinyl phenol) (PVP), poly(styrene-*co*-allyl alcohol) (PSA), and poly(bisphenol A-*co*-epichlorohydrin) (PBE) using spin coating. These thin films were characterized in terms of their transmittance, pencil hardness, and surface morphologies. The transmittance values of the PVP hybrid thin films decreased with the addition of TiOPPh because of the formation of Ti–O–Ph bonds. The pencil hardness values of the hybrid thin films were in the order PVP > PBE > PSA hybrids. Using confocal laser scanning microscopy and atomic force microscopy, the pencil hardness values were determined to be strongly dependent on the surface morphology, such as the roughness and presence of pin holes. The model cluster was synthesized by the reaction of TiOPPh with excess ethanol to study the structures of the TiOPPh in hybrids. From the nuclear magnetic resonance spectroscopy and single-crystal X-ray structure analyses, the main core structure of the model cluster was found to retain the core structure of TiOPPh.

Introduction

Organic–inorganic hybrid materials containing elemental blocks, a structural unit consisting of various groups of elements [1], have been developed in the field of material chemistry because they show excellent performance such as improved mechanical and thermal stabilities [2], gas permeability [3], and optical and emission properties [2, 4, 5]. As element blocks, polyhedral oligomeric silsesquioxanes (POSS blocks) [1, 6, 7], which are composed of silicon and oxygen atoms, and titanium-oxo clusters [8–10], which are composed of titanium and oxygen atoms, are well known. These element blocks are more desirable inorganic molecules compared with inorganic nanoparticles because of their high solubility in organic solvents, uniformity of size and shape, and easy purification [11–13]. Moreover, the reactivities of these element blocks are lower than those of metal salts such as $TiCl_4$ and $Ti(O\mathit{i}Pr)_4$, and they are easier to handle. For titanium-oxo clusters, Sanchez [14, 15] and Schubert [16, 17] prepared organic–inorganic hybrids that showed improved thermal stability. However, the synthesis of these clusters requires delicate techniques to prevent the facile decomposition (in particular, small clusters with fewer than 10 titanium atoms readily collapse) [18, 19] and circumvent their poor solubility in organic solvents. Therefore, we have focused and studied titanium phosphonate clusters as a new element block because the cluster can be easily synthesized by the reaction of titanium tetraisopropoxide with organic phosphonic acid at room temperature. Titanium phosphonate clusters having alkoxyl groups, first reported by Mutin et al. [20, 21], are composed of phosphatitanoxane bonds (Ti–O–P), which

Electronic supplementary material The online version of this article (https://doi.org/10.1038/s41428-018-0108-9) contains supplementary material, which is available to authorized users.

✉ Takahiro Gunji
gunji@rs.noda.tus.ac.jp

[1] Department of Pure and Applied Chemistry, Faculty of Science and Technology, Tokyo University of Science, 2641 Yamazaki, Noda, Chiba 278-8510, Japan

[2] Advanced Automotive Research Collaborative Laboratory, Graduate School of Engineering, Hiroshima University, 1-4-1 Kagamiyama, Higashi-Hiroshima City, Hiroshima 739-8527, Japan

are well known to have high chemical and thermal stabilities [22, 23]. These clusters can be incorporated into organic–inorganic hybrid materials using a sol–gel reaction or transalkoxylation because they contain alkoxyl groups. We previously reported the preparation and properties of free-standing films and thin films of organic–inorganic hybrid materials containing $[Ti_4(\mu_3\text{-O})(O\mathit{i}Pr)_5(\mu\text{-}O\mathit{i}Pr)_3(O_3PPh)_3]\cdot THF$ (TiOPPh) using various organic polymers. Accordingly, the mechanical properties, thermal properties, transmittance values, and refractive indices of some organic–inorganic hybrid materials were observed to be superior to those of the original organic polymers [24, 25]. In particular, the hybrid materials formed by covalent bonding between hydroxyl-substituted polymers and TiOPPh showed excellent performances. However, it remained uncertain why the mechanical properties decreased with increasing concentration of the cluster; therefore, close study of this phenomenon is necessary.

In this work, we prepared organic–inorganic hybrid thin films containing TiOPPh based on hydroxyl-substituted organic polymers (PVP: poly(vinyl phenol), PSA: poly (styrene-*co*-allyl alcohol), and PBE: poly(bisphenol A-*co*-epichlorohydrin)) as shown in Scheme 1. These hybrid films were characterized in terms of their FT-IR spectra, transmittance values, and surface morphologies. These hybrid thin films were examined by pencil hardness to determine the relationship between their surface morphologies and mechanical properties. Moreover, the model cluster was synthesized and characterized using nuclear magnetic resonance (NMR) spectroscopy, and its structure in the organic–inorganic hybrid materials was analyzed.

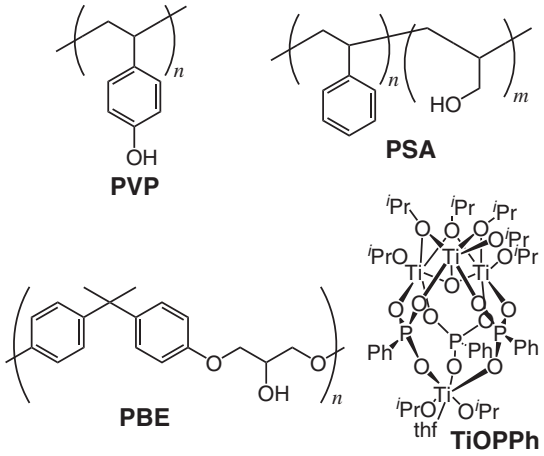

Scheme 1 Chemical structures of the polymers and TiOPPh

Experimental procedures

Measurements

NMR spectra were recorded using a JEOL Resonance JNM-ECP 500 spectrometer (JEOL, Akishima, Japan) (^{1}H at 500.16 MHz, ^{13}C at 125.77 MHz, and ^{31}P at 202.46 MHz) at 24 °C. The chemical shifts are reported in p.p.m. relative to chloroform-*d* ($CDCl_3$), which was used as an internal standard (for ^{1}H: 7.26 p.p.m. in residual chloroform, for ^{13}C: 77.00 p.p.m.). The ^{31}P NMR spectra were recorded using 85% phosphoric acid as an external standard. Fourier transform infrared (FT-IR) spectra were recorded using an FT/IR-6100 spectrophotometer (JASCO, Hachioji, Japan) by coating films onto a silicon wafer. Transmittance spectra were recorded using a JASCO V-670 spectrophotometer equipped with an integrating-sphere photometer ISN-470 type (JASCO, Hachioji, Japan) in the 300–800 nm wavelength range by coating films onto glass substrates. The hardness of the surfaces was evaluated via pencil hardness tests using a No. 553-M Pencil Scratch Hardness Tester (YASUDA, Nishinomiya, Japan) and subsequently using a JIS K5400, in which a vertical force of 10 N was applied at an angle of 45° to the horizontal film surface with a pencil. The obtained hardness values were evaluated using the hardness values of "Mitsubishi Uni pencils." Confocal laser scanning microscopy (CLSM) observations were obtained using a Color Laser 3D Profile Microscope VK-8510 (KEYENCE, Osaka, Japan). Atomic force microscopy (AFM) observations were obtained using an SPM-9700 instrument (Shimadzu, Kyoto, Japan). Differential scanning calorimetry (DSC) was performed using a DSC 3500 Sirius instrument (Netzsch Japan, Yokohama, Japan). Heating was performed at the rate of 5 °C/min under a nitrogen flow, and thereafter cooling was performed at a rate of 5 °C/min until a temperature of 50 °C was reached. This process was repeated three times. X-ray diffraction (XRD) patterns were recorded using an IC Vario instrument (PANalytical, Tokyo, Japan) with monochromatic Cu Kα radiation as the X-ray source. Small-angle X-ray scattering (SAXS) measurements were recorded using a SAXSess camera (Anton Paar Japan, Shinagawa, Japan) equipped with a PANalytical PW3830 laboratory X-ray generator with Cu Kα radiation (0.154 nm, 40 kV, 50 mA) as the X-ray source.

Crystal data were collected using a Bruker AXS SMART APEX CCD X-ray diffractometer equipped with a monochromatic Mo Kα radiation soure (0.7107 Å). Empirical absorption corrections using equivalent reflections and Lorentzian polarization corrections were performed using the SADABS program [26]. All data were collected using SMART and Bruker SAINTPLUS (Version 6.45) software packages. The structures were analyzed using the SHELXA-97 program [27] and refined against F^2 by using SHELEXL-97 [28].

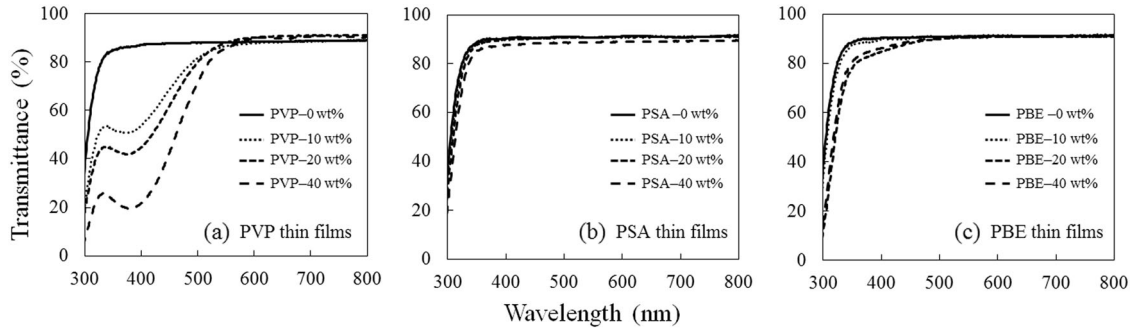

Fig. 1 UV–Vis transmission spectra of the **a** PVP, **b** PSA, and **c** PBE thin films

Materials

All the solvents were purified using a standard process [29] and stored over activated molecular sieves. PVP ($M_w = 25{,}000$ g/mol), PSA ($M_w = 2200$ g/mol, allyl alcohol 40 mol%), and PBE ($M_w = 40{,}000$ g/mol) were purchased from Sigma–Aldrich (Tokyo, Japan) and used as received. $[Ti_4(\mu_3\text{-O})(O\mathit{i}Pr)_5(\mu\text{-}O\mathit{i}Pr)_3(O_3PPh)_3]\cdot$THF (TiOPPh) was prepared as described previously [24, 30] and characterized as shown in the supporting information. The glass substrate (S9112) and silicon wafers (4″ polishing wafer) were purchased from Matsunami Glass Ind. and GlobalWafers Co., Ltd., respectively. These substrates were cut to 2.5 cm × 2.5 cm and cleaned three times via ultrasonication in acetone.

Preparation of organic–inorganic hybrid thin films

The precursors were prepared by mixing polymers (0.125 g) and TiOPPh in 5 mL of tetrahydrofuran (THF) for 3 h at room temperature. These precursors were dropped onto the silicon wafer or glass substrate and spun at a rate of 3000 r.p.m. for 20 s, and then dried at 110 °C for 10 min. This process was repeated twice.

The samples are abbreviated using the polymer name and the concentration of TiOPPh in weight percent, e.g., PVP–40 wt%.

Synthesis of model cluster (compound 1)

TiOPPh (0.2 g, 160 µmol) was dissolved in excess hot EtOH (5 mL, 86 mmol) in a glove box. The solution was cooled to room temperature and maintained for several days. The model cluster (compound **1**) was obtained as colorless crystals (20 mg, 11%).

$^{13}C\{^1H\}$ NMR (126 MHz, $CDCl_3$/77.00 p.p.m.): $\delta =$ 17.79, 18.12, 18.34, 70.32, 71.12, 71.87, 127.24 (d, $^2J_{C-P} =$ 14.4 Hz), 129.72, 131.43 (d, $^3J_{C-P} = 9.7$ Hz), 134.86 (d, $^1J_{C-P} = 201$ Hz).

$^{31}P\{^1H\}$ NMR (202 MHz, $CDCl_3$/ p.p.m.): $\delta = 8.7$.

Results and discussion

Preparation of hybrid thin films

The thin hybrid films were prepared via spin-coating onto the substrate (silicon wafer or glass) by dropping the precursor prepared by mixing TiOPPh and polymer in THF. These hybrid films were characterized using FT-IR spectroscopy; the intensity of the hydroxyl group stretching vibration in the polymer decreased with the addition of TiOPPh because transalkoxylation occurred between the polymer and TiOPPh.

The transmittance values of the thin films on glass substrates are shown in Fig. 1 and Table 1. For the PVP hybrid thin films, the transmittance decreased with increasing concentration of TiOPPh, and the films became orange-red. The color development is attributed to the ligand-to-metal charge transfer due to the formation of Ti–O–Ph bonds as observed in the orange-red crystals of $[Ti_2(\mu\text{-}OPh)_2(OPh)_6(HOPh)_2]$ [31, 32]. For the PSA hybrid thin films, the transmittance was high even at 40 wt% content of TiOPPh. The transmittance of the PBE hybrid thin films slightly decreased with increasing TiOPPh content in the short visible range. We propose that the decrease in transmittance is caused by the ligand-to-metal charge transfer based on the coordination of the ether groups in PBE to the titanium atoms [25].

Glass transition temperatures of the hybrids

The glass transition temperatures (T_g values) of the PVP and PBE hybrid films were measured using DSC (Fig. 2). The T_g values of pure PVP, PSA, and PBE were 184, 63, and 98 °C, respectively. The T_g values of the hybrid materials were higher than those of the pure polymers, and only one peak was observed for each of the PVP hybrids; the T_g values of PVP–20 wt% and PVP–40 wt% were 226 and >250 °C, respectively. The T_g values of PSA–20 wt% and PSA–40 wt% were 67 and 76 °C, respectively. The T_g of PBE–20 wt% was 112 °C, and the glass transition of

Table 1 Transmittance and pencil hardness values of the hybrid thin films

Content of cluster **1** (wt%)	Transmittance[a] (%)	Hardness[b]
PVP		
0	87	4B
10	59	H
20	50	2H
40	28	HB
PSA		
0	91	5B
10	90	5B
20	90	4B
40	88	6B
PBE		
0	90	2B
10	90	4B
20	86	HB
40	87	B

The hardness increases in the order

6B < 5B < 4B < 3B < 2B < B < HB < F < H < 2H

[a]Measured using UV–Vis spectrometry at 420 nm

[b]Measured using pencil hardness tests

PBE–40 wt% was not observed even at 140 °C. Thus, TiOPPh strongly inhibited the mobility of the polymers, and these films were hybrids between the polymers and TiOPPh because the T_g values of the films were higher than those of the pure polymers [16, 17, 33–35].

Surface morphologies of the hybrid thin films

The micro-scale surface morphologies of the hybrids were observed using CLSM as shown in Fig. 3. The PVP and PSA hybrids showed flat surfaces; therefore, TiOPPh caused no macro-aggregation. On the other hand, the PBE hybrids showed microphase separations similar to that seen in copolymers containing POSS [36] and poly(methylsilsesquioxane-*co*-siloxane) [37]. The formation of microphase separation at the micro scale was similar to that seen in nano-TiO_2 hybrids based on bisphenol A-epoxy [38]; hence, the bisphenol A-based hybrids may undergo microphase separation. Additionally, PBE–40 wt% was confirmed to have very small white dots. The protuberances looked like branches of a tree and are shown in Fig. 3j, k. The features are formed by the aggregation of clusters bound to PBE because of the high concentration of TiOPPh relative to that of PBE.

The nanoscale surface morphologies of the PVP, PSA, and PBE hybrid films were observed using AFM. The surface of the PVP–20 wt% film was uniform and smooth,

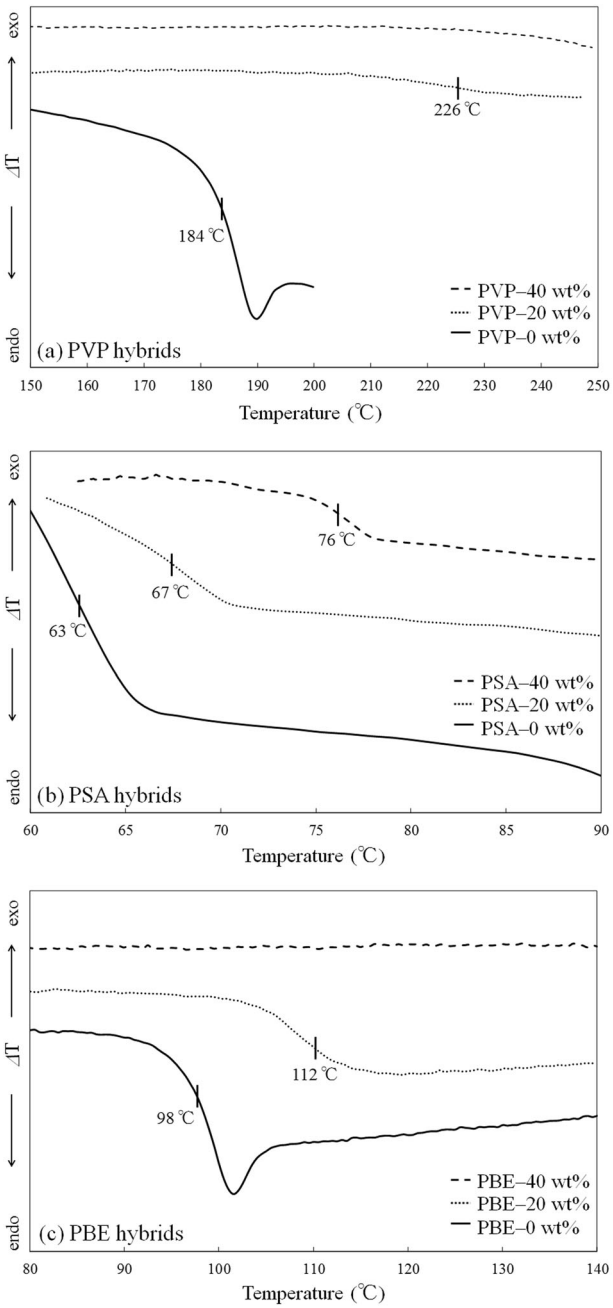

Fig. 2 DSC traces of the **a** PVP, **b** PSA, and **c** PBE hybrids

although some pin holes were observed (Fig. 4a). Surprisingly, the surface of the PVP–40 wt% film showed many large pin holes with diameters of 30–70 nm as shown in Fig. 4b. The surface of the PSA–20 wt% film was slightly rough compared to that of the PVP–20 wt% film (Fig. 4c), and the surface of the PSA–40 wt% film showed many pin holes. The surfaces of the PBE hybrids were rough and showed many pin holes even with the addition of 20 wt% TiOPPh (Fig. 4e, f). The PVP–20 wt% and PSA–20 wt% films were homogeneous. For other hybrids, the formation of pin holes might be caused by the formation of

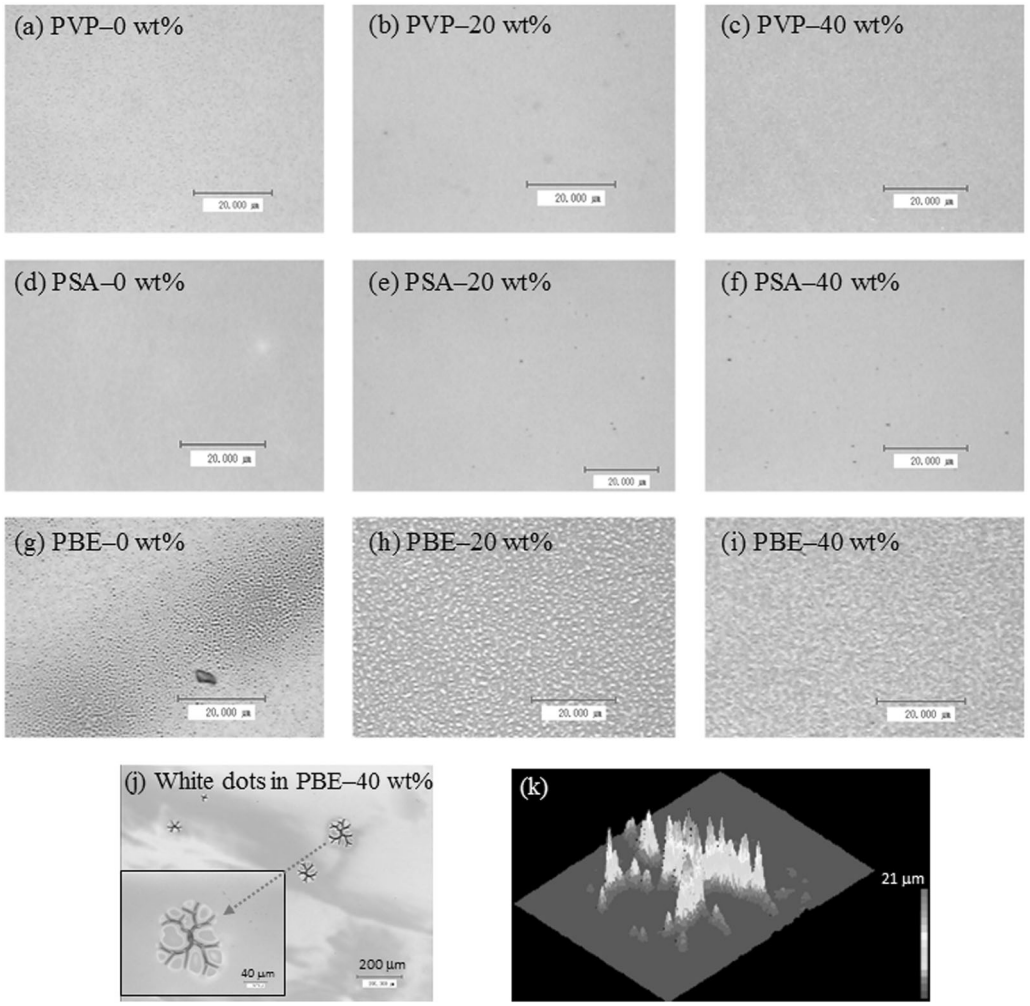

Fig. 3 CLSM images of the **a**–**c** PVP, **d**–**f** PSA, and **g**–**i** PBE thin films; **j**, **k** white dots in PBE–40 wt%

microphase separation [39–42], which is caused by nanoaggregation of TiOPPh in polymer–40 wt% hybrids, the formation of lamellar structures such as those seen in poly(styrene-*co*-methyl methacrylate) [41, 42], and/or volatilization of organic compounds (THF and *i*PrOH) due to the increased viscosity in the solution of polymer–40 wt %. Based on AFM observations over large areas (5 μm × 5 μm), the formation of pin holes was observed in the whole film. Additionally, PVP hybrids were evaluated by SAXS; however, the characteristic pattern generated by lamellar structures was not observed. From these results, the formation of pin holes was caused by the microphase separation of TiOPPh domains due to the high concentration of TiOPPh relative to the concentration of polymer.

Surface hardness of the hybrid thin films

The results of the pencil hardness test are shown in Fig. 5 and Table 1. The hardness of the PVP hybrid thin films increased with the addition of TiOPPh, and the thin film with 20 wt% TiOPPh showed the greatest hardness (2H). However, the hardness of the thin film with 40 wt% TiOPPh was lower than those of the thin films with 10 and 20 wt% TiOPPh. The PBE hybrid thin films were slightly influenced by the addition of TiOPPh, but the hardness values of the PBE hybrid thin films were lower than those of the PVP hybrid thin films. The conversion rate between the TiOPPh and PBE matrices might be lower than that between TiOPPh and PVP because Ti–O–Ph bonds are stronger and more easily formed than Ti–O–alkyl bonds [43] depending on the pK_a and sterics of the alcohol [44]. Additionally, the surface roughness must be influenced by the presence of microphase separation on the micro scale. However, the hardness values of the PSA hybrid thin films did not change substantially. We attribute the lack of improvement in the hardness values of the PSA hybrid thin films to the reduced transalkoxylation, which is caused by the steric hindrance and/or rigid structure from the π–π interactions of the

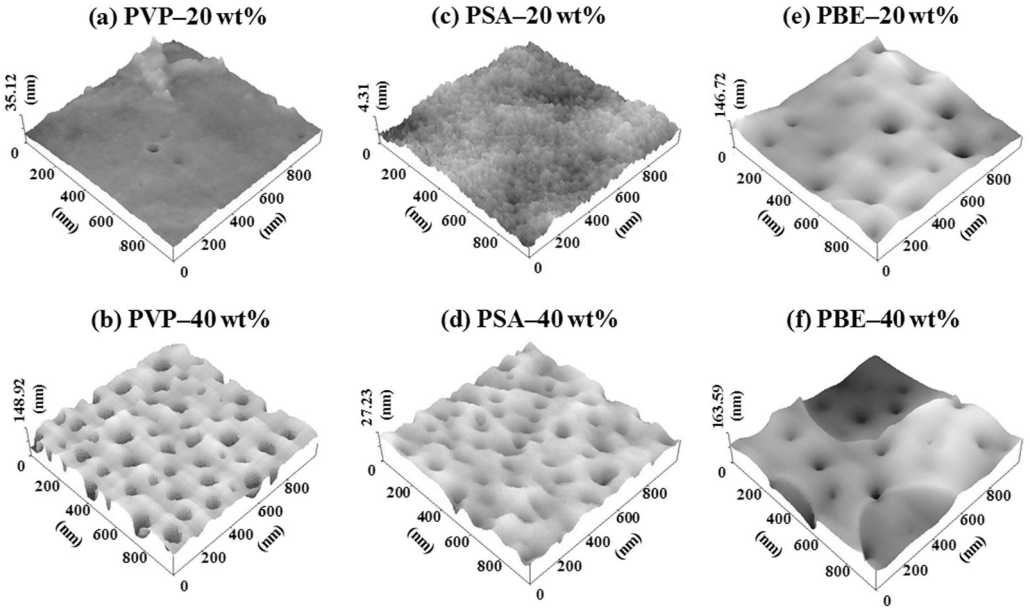

Fig. 4 AFM images of the PVP, PSA, and PBE hybrid thin films

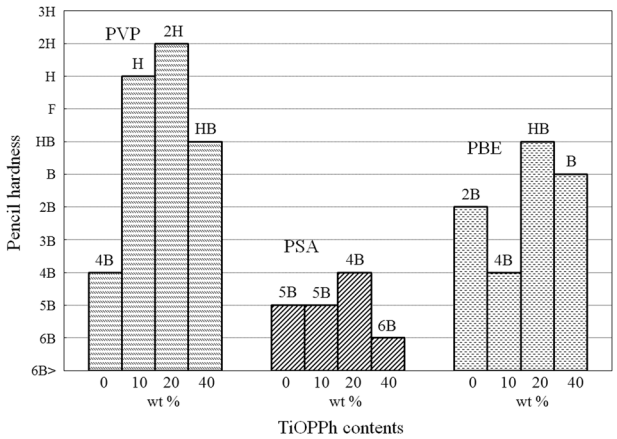

Fig. 5 Pencil hardness values of the PVP, PSA, and PBE hybrid thin films

polystyrene domains. The pencil hardness is known to be dependent on the degree of crosslinking, surface smoothness, and adhesion to the substrate [45, 46]. From the increase in T_g values observed using DSC, the degree of crosslinking can be concluded to increase with increasing TiOPPh content. However, the surface morphologies of the hybrid thin films containing 40 wt% TiOPPh were rough and showed the formation of pin holes. Therefore, the lower pencil hardness values for hybrids with 40 wt% TiOPPh were strongly influenced by the surface smoothness and, in particular, the formation of pin holes. The presence of micro-scale aggregates, such as those seen in PBE–40 wt%, also decreased the surface hardness.

Synthesis and characterization of compound 1

We synthesized the model cluster (compound **1**) to study the structure of TiOPPh in the polymer. Compound **1** was synthesized by the reaction of TiOPPh with hot EtOH. The ^{31}P NMR spectrum of the reaction solution showed a singlet signal at 8.8 p.p.m. After a few days, colorless crystals of compound **1** were obtained from the solution. In the ^{31}P NMR spectrum of compound **1** in $CDCl_3$, a singlet signal was observed at 8.7 p.p.m., and the chemical shift of compound **1** was similar to that of the reaction solution. Therefore, compound **1** was determined to be the major product of the reaction. The ^{13}C NMR spectra of TiOPPh and compound **1** are shown in Fig. 6. The ^{13}C NMR spectrum of TiOPPh showed signals assigned to a phenyl group (at 127.3–134.4 p.p.m.), a coordinated THF molecule (at 25.4 and 68.8 p.p.m.), a bridged isopropoxyl group (at 24.8 and 79.4 p.p.m.), and terminal isopropoxyl groups (at 24.5, 24.8, and 78.5 p.p.m.). The spectrum of compound **1** showed signals attributable to phenyl groups and bridged and terminal ethoxyl groups, and no signals that could be attributed to isopropoxyl groups and a coordinated THF molecule. Compound **1** was analyzed using X-ray crystallography, but it was very sensitive to moisture. Therefore, the structure refinement of compound **1** converged at a very high *R* factor, and the structure of compound **1** was similar to that of TiOPPh (see supporting information). Thus, compound **1** was converted to $[Ti_4(\mu_3\text{-}O)(OEt)_5(\mu\text{-}OEt)_3(O_3PPh)_3]\cdot EtOH$ by the exchange of the isopropoxyl groups with ethoxyl groups. Hence, the core structure of the cluster in the hybrid materials is retained.

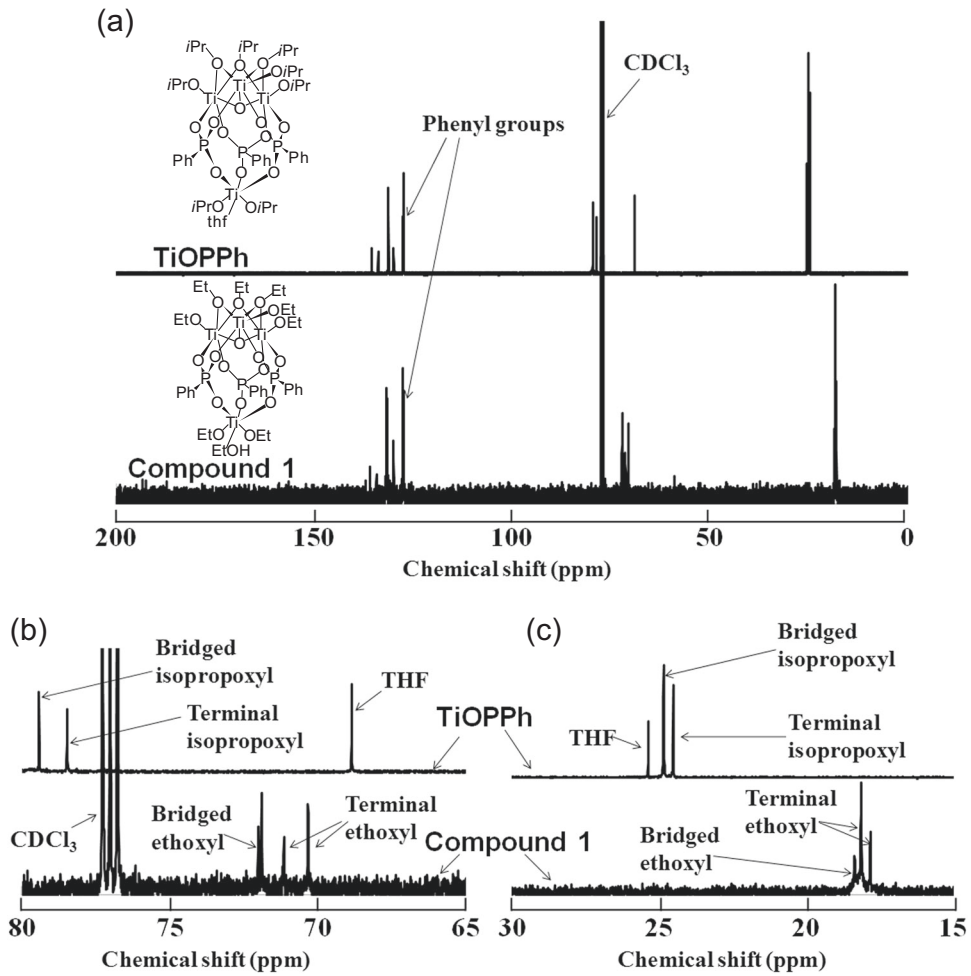

Fig. 6 ^{13}C NMR spectra of TiOPPh and compound **1**: **a** region 0–200 p.p.m., **b** region 65–80 p.p.m., and **c** region 15–30 p.p.m.

Conclusion

Organic–inorganic hybrid thin films containing TiOPPh were prepared via the hybridization of TiOPPh with PVP, PSA, and PBE using spin coating. The success of the hybridization was confirmed by FT-IR spectroscopy and DSC. The transmittance values of the PVP hybrid thin films decreased with the addition of TiOPPh because of the appearance of an absorption band for the ligand-to-metal charge transfer due to the formation of Ti–O–Ph bonds. The transmittance values of other hybrids were high. The PVP–20 wt% thin film showed a uniform and smooth surface, but the surface of the PVP–40 wt% thin film was confirmed to have many pin holes, which is similar to that seen for PSA hybrids. For the PBE hybrid thin film, the surface was rough, and the pin holes observed in the film with 40 wt% TiOPPh were larger and more abundant compared to those observed in the film containing 20 wt% TiOPPh. The formation of pin holes might be caused by microphase separations or the elimination of solvent. The pencil hardness values of the hybrid thin films improved in the order PVP > PBE > PSA; notably, the pencil hardness of PVP–20 wt% was the highest (2 H). TiOPPh acted as a good cross-linker because transalkoxylation occurred between TiOPPh and the polymer. Moreover, hardness values of the hybrid thin films increased in the order of TiOPPh concentration 20 wt% > 40 wt% > 0 wt% due to the degree of crosslinking, surface smoothness, and adhesion to the substrate in each sample.

Compound **1**, as a model cluster, was synthesized by the reaction of TiOPPh with excess ethanol. From NMR spectroscopy and single-crystal X-ray structure analyses, the structure of compound **1** was characterized as $[Ti_4(\mu_3\text{-}O)(OEt)_5(\mu\text{-}OEt)_3(O_3PPh)_3]\cdot EtOH$ due to the exchange of the isopropoxyl groups of TiOPPh with ethoxyl groups. Therefore, we suggest that the core of TiOPPh is retained in the hybrid polymers.

Acknowledgements This work was supported by a Grant-in-Aid for Scientific Research on Innovative Areas "New Polymeric Materials Based on Element-Blocks" (No. 2401) (JSPS KAKENHI Grant Number JP24102008). This work was also supported by JSPS KAKENHI Grant Number JP16K17951. Mr. Keigo Kurokawa, Mr. Masahiro Ohashi, and Mr. Yudai Suzuki are greatly appreciated for their assistance with the SAXS measurements and DSC analyses.

Compliance with ethical standards

Conflict of interest The authors declare that they have no conflict of interest.

References

1. Chujo Y, Tanaka K. New polymeric materials based on element-blocks. Bull Chem Soc Jpn. 2015;88:633–43.
2. Tanaka K, Yamane H, Mitamura K, Watase S, Matsukawa K, Chujo Y. Transformation of sulfur to organic–inorganic hybrids employed by networks and their application for the modulation of refractive indices. J Polym Sci, Part A: Polym Chem. 2014;52:2588–95.
3. Kanezashi M, Shioda T, Gunji T, Tsuru T. Gas permeation properties of silica membranes with uniform pore sizes derived from polyhedral oligomeric silsesquioxane. AIChE J. 2012;58:1733–43.
4. Fujita M, Idota N, Matsukawa K, Sugahara Y. Preparation of oleyl phosphate-modified TiO_2/poly(methyl methacrylate) hybrid thin films for investigation of their optical properties. J Nanomater. 2015;2015:1–8.
5. Yamane H, Ito S, Tanaka K, Chujo Y. Preservation of main-chain conjugation through BODIPY-containing alternating polymers from electronic interactions with side-chain substitutents by cardo boron structures. Polym Chem. 2016;7:2799–807.
6. Tanaka K, Chujo Y. Advanced functional materials based on polyhedral oligomeric silsesquioxane (POSS). J Mater Chem. 2012;22:1377–746.
7. Cordes DB, Lickiss PD, Rataboul F. Recent developments in the chemistry of cubic polyhedral oligosilsesquioxanes. Chem Rev. 2010;110:2081–173.
8. Rozes L, Sanchez C. Titanium oxo-clusters: precursors for a Lego-like construction of nanostructured hybrid materials. Chem Soc Rev. 2011;40:1006–30.
9. Schubert U. Organofunctional metal oxide clusters as building blocks for inorganic–organic hybrid materials. J Sol–Gel Sci Technol. 2004;31:19–24.
10. Rozes L, Steunou N, Fornasieri G, Sanchez C. Titanium-oxo clusters, versatile nanobuilding blocks for the design of advanced hybrid materials. Mon Chem. 2006;137:501–28.
11. Schubert U. Inorganic–organic hybrid polymers based on surface-modified metal oxide clusters. Macromol Symp. 2008; 267:1–8.
12. Gross S. Oxocluster-reinforced organic–inorganic hybrid materials: effect of transition metal oxoclusters on structural and functional properties. J Mater Chem. 2011;21:15853–61.
13. Schubert U. Cluster-based inorganic–organic hybrid materials. Chem Soc Rev. 2011;40:575–82.
14. Rozes L, Fornasieri G, Trabelsi S, Creton C, Zafeiropoulos NE, Stamm M, et al. Reinforcement of polystyrene by covalently bonded oxo-titanium clusters. Prog Solid State Chem. 2005;33:127–35.
15. Bocchini S, Fornasieri G, Rozes L, Trabelsi S, Galy J, Zafeiropoulos NE, et al. New hybrid organic–inorganic nanocomposites based on functional $[Ti_{16}O_{16}(OEt)_{24}(OEMA)_8]$ nano-fillers. Chem Commun. 2005;2600-2.
16. Moraru B, Hüsing N, Kickelbick G, Schubert U, Fratzl P, Peterlik H. Inorganic–organic hybrid polymers by polymerization of methacrylate- or acrylate-substituted oxotitanium clusters with methyl methacrylate or methacrylic acid. Chem Mater. 2002;14:2732–40.
17. Gao Y, Choudhury NR, Matisons J, Schubert U, Moraru B. Part 2: inorganic–organic hybrid polymers by polymerization of methacrylate-substituted oxotitanium clusters with methyl methacrylate: thermomechanical and morphological properties. Chem Mater. 2002;14:4522–9.
18. Day VW, Eberspacher TA, Chen Y, Hao J, Klemperer WG. Low-nuclearity titanium oxoalkoxides: the trititanates $[Ti_3O](OPr^i)_{10}$ and $[Ti_3O](OPr^i)_9(OMe)$. Inorg Chim Acta. 1995;229:391–405.
19. Chen YW, Klemperer WG, Park CW. Polynuclear titanium oxoalkoxides: molecular building blocks for new materials? Mater Res Soc Symp Proc. 1992;271:57–64.
20. Guerrero G, Mehring M, Mutin PH, Dahan F & Vioux A. Syntheses and single-crystal structures of novel soluble phosphonate- and phosphinato-bridged titanium oxo alkoxides. J Chem Soc, Dalton Trans. 1999;1537-8.
21. Mehring M, Guerrero G, Dahan F, Mutin PH, Vioux A. Syntheses, characterizations, and single-crystal X-ray structures of soluble titanium alkoxide phosphonates. Inorg Chem. 2000;39:3325–32.
22. Sanchez C, Belleville P, Popall M, Nicole L. Applications of advanced hybrid organic–inorganic nanomaterials: from laboratory to market. Chem Soc Rev. 2011;40:696–753.
23. Guerrero G, Mutin PH, Vioux A. Anchoring of phosphonate and phosphinate coupling molecules on titania particles. Chem Mater. 2001;13:4367–73.
24. Hayami R, Wada K, Sagawa T, Tsukada S, Watase S, Gunji T. Preparation and properties of organic–inorganic hybrid polymer films using $[Ti_4(\mu_3\text{-}O)(O^iPr)_5(\mu\text{-}O^iPr)_3(O_3PPh)_3]$·thf. Polym J. 2017;49:223–8.
25. Hayami R, Wada K, Nishikawa I, Sagawa T, Tsukada S, Yamamoto K, et al. Preparation and properties of organic–inorganic hybrid materials using titanium phosphonate cluster. Polym J. 2017;49:665–9.
26. Sheldrick GM. SADABS, program for Siemens area detector absorption correction. Germany: University of Göttingen; 1996.
27. Sheldrick GM. SHELXS-97, program for crystal structure solution. Germany: University of Göttingen; 1997.
28. Sheldrick GM. SHELXL-97, program for crystal structure refinement. Germany: University of Göttingen; 1997.
29. Armarego WLF, Chai C. Purification of laboratory chemicals. 7th Ed. Oxford, UK: Elsevier; 2012.
30. Hayami R, Sagawa T, Tsukada S, Yamamoto K, Gunji T. Synthesis, characterization and properties of titanium phosphonate clusters. Polyhedron. 2018;147:1–8.
31. Svetich, GW & Voge, AA Crystal molecule structure of tetraphenoxytitanium(IV) monophenolate, $Ti(OPh)_4$, HOPh. J Chem Soc. 1971;D 676-7.
32. Svetich GW, Voge AA. The crystal and molecular structure of *sym-trans*-di-μ-phenoxyhexaphenoxydiphenolatodititanium (IV). Acta Crystallogr B. 1972;28:1760–7.
33. Otsuka T, Chujo Y. Poly(methyl methacrylate) (PMMA)-based hybrid materials with reactive zirconium oxide nanocrystals. Polym J. 2010;42:58–65.
34. Kim K.-M, Keum D.-K, Chujo Y. Organic–inorganic polymer hybrdis using polyoxazoline initiated by functionalized silsesquioxane. Macromolecule. 2003;36:867–75.
35. Kameneva O, Kuznestov AI, Smirnova LA, Rozes L, Sanchez C, Alexandrov A, et al. New photoactive hybrid organic–inorganic materials based on titanium-oxo-PHEMA nanocomposites exhibiting mixed valence properties. J Mater Chem. 2005;15:3380–3.
36. Pyun J, Matyjaszewski K, Wu J, Kim G.-M, Chun SB, Mather PT. ABA triblock copolymers containing polyhedral oligomeric silsesquioxane pendant groups: synthesis and unique properties. Polym (Guildf). 2003;44:2739–50.
37. Gunji T, Kaburagi H, Tsukada S, Abe Y. Preparation, properties, and structure of polysiloxanes by acid-catalyzed controlled hydrolytic co-polycondensation of polymethyl(methoxy)siloxane and polymethoxysiloxane. J Sol–Gel Sci Technol. 2015;75:564–73.

38. Tercjak A, Gutierrez J, Peponi L, Rueda L, Mondragon I. Arrangement of conductive TiO2 nanoparticles in hybrid inorganic/organic thermosetting materials using liquid crystal. Macromolecules. 2009;42:3386–90.
39. Liu Y. Polymerization-induced phase separation and resulting thermomechanical properties of thermosetting/reactive nonlinear polymer blends: A review. J Appl Polym Sci. 2013;127:3279–92.
40. Zeng L, Zhao TS. An effective strategy to increase hydroxide-ion conductivity through microphase separation induced by hydrophobic-side chains. J Power Sources. 2016;303:354–62.
41. Farrell RA, Fitzgerald TG, Borah D, Holmes JD, Morris MA. Chemical interactions and their role in the microphase separation of block copolymer thin films. Int J Mol Sci. 2009;10:3671–712.
42. Green PF, Limary R. Block copolymer thin films: pattern formation and phase behavior. Adv Colloid Interface Sci. 2001;94:53–81.
43. Fornasieri G, Rozes L, Le Calvé S, Alonso B, Massiot D, Rager MN, et al. Reactivity of titanium oxo ethoxo cluster $[Ti_{16}O_{16}(OEt)_{32}]$. Versatile precursor of nanobuilding block-based hybrid materials. J Am Chem Soc. 2005;127:4869–78.
44. Bradley DC, Mehrotra RC, Rothwell IP, Singh A. Alkoxo and aryloxo derivatives of metals. San Diego, USA: Academic Press; 2001.
45. Tadanaga K, Azuta K, Minami T. Preparation of organic–inorganic hybrid coating films from vinyltriethoxysilane–tetraethoxysilane by the sol–gel method. J Ceram Soc Jpn. 1997;105:555–8.
46. Takamura N, Okonogi H, Gunji T, Abe Y. Preparation and properties of polysilsesquioxanes –preparation and properties of polymer hybrids from vinyltrimethoxysilane–. Kobunshi Ronbunshu. 2000;57:198–207.